



## OPEN ACCESS

## EDITED BY

Adelina Geyer,  
Spanish National Research Council  
(CSIC), Spain

## REVIEWED BY

Ian Ernest Masterman Smith,  
The University of Auckland,  
New Zealand  
Javier Dóniz-Páez,  
University of La Laguna, Spain  
Pablo Grosse,  
Consejo Nacional de Investigaciones  
Científicas y Técnicas (CONICET),  
Argentina

## \*CORRESPONDENCE

Joseph A. Nolan,  
janolan@protonmail.com

## SPECIALTY SECTION

This article was submitted to  
Volcanology,  
a section of the journal  
Frontiers in Earth Science

RECEIVED 31 March 2022

ACCEPTED 18 July 2022

PUBLISHED 21 September 2022

## CITATION

Nolan JA and Graettinger AH (2022),  
Small-volume monogenetic igneous  
landforms and edifices statistics  
(SMILES): A catalog of representative  
mafic volcanic landforms to enable  
quantitative remote identification.  
*Front. Earth Sci.* 10:910107.  
doi: 10.3389/feart.2022.910107

## COPYRIGHT

© 2022 Nolan and Graettinger. This is an  
open-access article distributed under  
the terms of the [Creative Commons  
Attribution License \(CC BY\)](https://creativecommons.org/licenses/by/4.0/). The use,  
distribution or reproduction in other  
forums is permitted, provided the  
original author(s) and the copyright  
owner(s) are credited and that the  
original publication in this journal is  
cited, in accordance with accepted  
academic practice. No use, distribution  
or reproduction is permitted which does  
not comply with these terms.

# Small-volume monogenetic igneous landforms and edifices statistics (SMILES): A catalog of representative mafic volcanic landforms to enable quantitative remote identification

Joseph A. Nolan\* and Alison H. Graettinger

University of Missouri–Kansas City, Kansas City, MO, United States

Accurate classification of terrestrial and non-terrestrial volcanic landforms requires a robust suite of morphometric parameters. The Small-volume Monogenetic Igneous Landforms and Edifices Statistics (SMILES) catalog contains the morphometric characterizations of mafic small-volume volcanic landforms and was created using uncrewed aerial system photogrammetry, open-source LiDAR, and digital elevation model repositories. This study analyzed 20 simple maars, 22 lava collapse features, 24 ring scoria cones, and 24 spatter landforms (fissure and point source spatter ramparts), using high-resolution (<0.1–5 m/pixel) digital elevation models to establish what dimensionless morphometric parameters enable remote identification of the studied landforms. Parameters include isoperimetric circularity, depth ratio (crater depth/major chord), interior slope angles, as well as crater to base ratios for the area, perimeter, and major chord lengths. Landforms were limited to a basal width of <2 km and <1 km<sup>3</sup> for scoria cones and spatter landforms, and a major chord of 2 km or less for lava collapse features and maars. Simple maars have an aspect ratio (AR) (>0.74), isoperimetric circularity (IC) (>0.90), interior slope angle (<47°), and depth ratio (<0.26) creating a distinct range of morphometric parameters. Lava collapse features exhibit wider variability in AR (0.26–0.95), IC (0.46–0.98), interior slope angle (up to 16–86°), and depth ratio (0.25–0.52). Scoria cone craters have a distinct range of AR (>0.54), IC (>0.81), interior slope angle (<34°), and lower depth ratio (<0.25). Spatter landforms have a wider range of variability in AR (0.25–0.94), IC (0.43–0.98), interior slope angle (<63°), and depth ratio (0.04–0.37). Scoria cones have lower crater/base area ratios and lower crater/base perimeter ratios than spatter landforms. This study demonstrates that while an individual parameter is not diagnostic for recognizing small-volume mafic volcanic landforms remotely, a suite of parameters is. The SMILES catalog demonstrates the value of evaluating populations of similar landforms using higher-resolution datasets to establish diagnostic suites of dimensionless parameters, to enable accurate and positive remote identification of volcanic landforms. The technique used in this study can be applied to other volcanic and non-volcanic landforms on Earth, as well as non-terrestrial targets.

## KEYWORDS

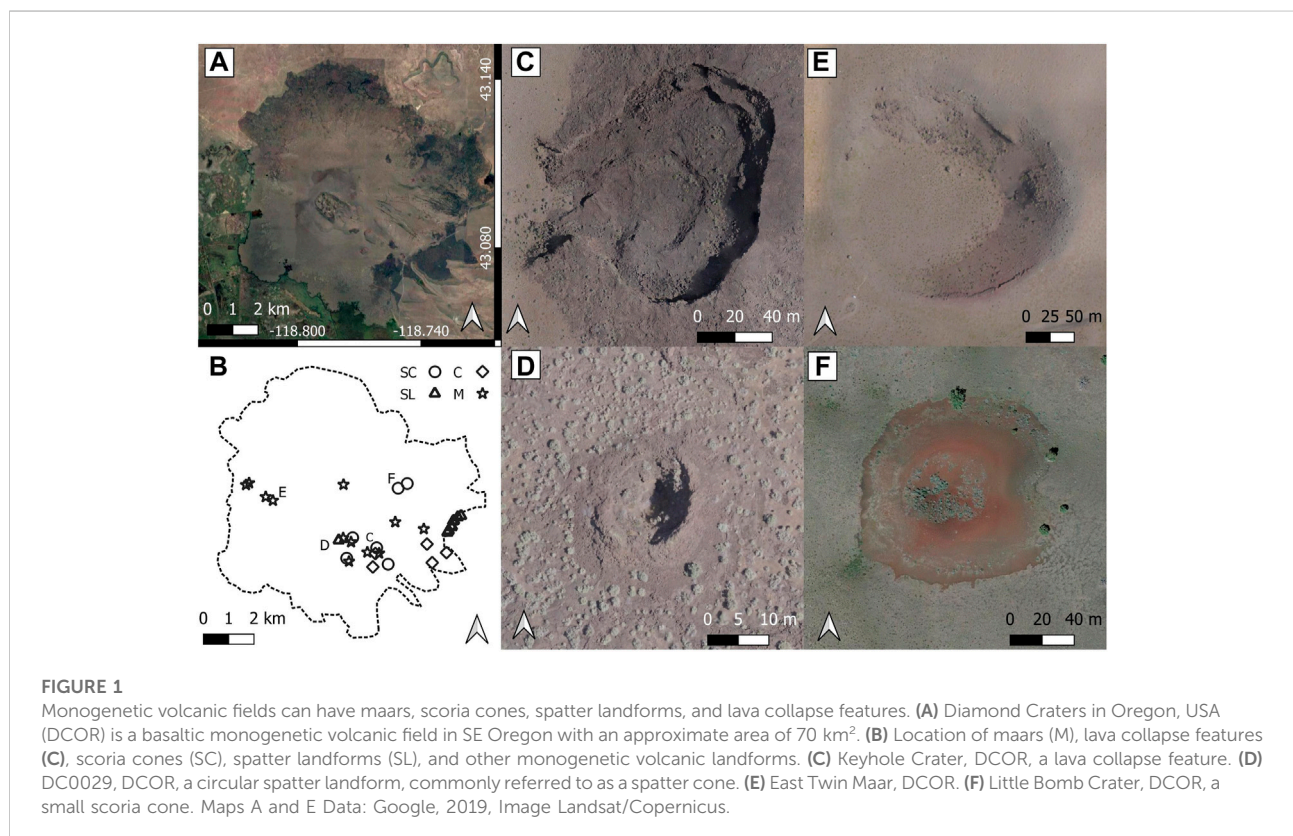
monogenetic volcanism, mafic volcanic, basaltic volcanic fields, monogenetic volcanic field, small-volume volcanoes

## Introduction

Most subaerial volcanoes on Earth and other planets occur in monogenetic basaltic volcanic fields (e.g., [Dóniz et al., 2008](#); [Valentine and Connor, 2015](#); [Valentine and Gregg, 2008](#); [Vespermann and Schmincke, 2000](#); [Wood, 1980](#)). The field may remain volcanically active for years to centuries, but the construction of individual landforms occurs through individual eruptive events, often referred to as monogenetic (e.g., [Marti et al., 2016](#); [Németh, 2010](#)). These monogenetic landforms are often small-volume (<1 km<sup>3</sup> total eruptive volume) ([Valentine et al., 2006](#); [Németh and Kereszturi, 2015](#); [Carracedo-Sánchez et al., 2017](#); [Aguilera et al., 2022](#)) and can be created through explosive magma/coolant interactions (phreatomagmatic), explosive magmatic, or effusive magmatic processes (e.g., [Canón-Tapia and Walker, 2004](#); [Murcia and Nemeth, 2016](#); [Smith and Németh, 2017](#)). Magmatic-dominated landforms include spatter landforms (both spatter cones and fissure ramparts), lava collapse features ([Greeley and Gault, 1979](#); [Sauro et al., 2020](#)), and scoria cones whereas phreatomagmatic processes create maars, tuff rings, and tuff cones. As an example, Diamond Craters, OR, (DCOR) is a basaltic monogenetic lava

field emplaced between 6,100 and 8,000 years ago covering ~70 km<sup>2</sup> in SE Oregon's desert ([Peterson and Groh, 1964](#); [Russell, 1987](#); [Sherrod et al., 2012](#)) ([Figure 1](#)). DCOR is home to monogenetic landforms ranging from 16 to 1,100 m in diameter produced by magmatic explosive and effusive, phreatomagmatic, and collapse processes. Similar to many monogenetic fields, DCOR is not built around a large central vent and was formed by regional extensional rifting ([Sherrod et al., 2012](#)). The presence of many different volcanic landform types in one field complicates remote classification. These difficulties increase when other landforms that may closely resemble volcanic features, such as lava collapse features, impact craters, or mud volcanoes, appear in the same field.

Monogenetic volcanic landforms (MVLs) are ideal for determining relations between morphometry and emplacement mechanisms due to the single, relatively short, eruption producing less complicated landforms ([Valentine et al., 2021](#)). However, MVL can exhibit more than one eruption mechanism such as phreatomagmatic to magmatic explosions during a single eruptive episode, hereby referred to as multimodal, and require an additional level of detail when quantifying (e.g., [Houghton and Schmincke, 1989](#); [Di Traglia](#)



et al., 2009). Examples include, but are not limited to, pyroclastic cones constructed inside a maar crater or a maar crater crosscutting a scoria cone. As a first step in evaluating the full spectrum of monogenetic volcanic landforms, the endmember landforms must be evaluated to establish the universal features related to a given eruption style. Consequently, this study investigated simple maars, a single, circular depression formed by phreatomagmatic explosion-dominated eruptions (Peterson and Groh, 1963; White and Ross, 2011; Graettinger, 2018). Similarly, only complete, single scoria cones formed primarily through magmatic processes, referred to as ring scoria cones, are included in this study (Dóniz-Páez, 2015; Bemis and Ferencz, 2017). Spatter cones and fissure ramparts are lumped in a single classification (spatter landforms) because the eruption mechanisms are the same, only the resulting morphology is different as a result of migrating loci of activity (Witt and Walter, 2017). The formation of spatter landforms results from dikes and the resulting morphology has rarely been addressed which means that there is no clear endmember case to study first and we study a range of available examples (Witt et al., 2018). Finally, lava collapse features were limited to those formed by the collapse of a lava flow surface as a result of a void. No classification was made between lava tube collapse (e.g., Sauro et al., 2020), dimple (drainage craters) (Greeley, 1970), or lava collapse depressions (Greeley and Gault, 1979).

The small-volume monogenetic igneous landforms and edifices statistics (SMILES) catalog contains the morphometric characterizations of maars, lava collapse features, scoria cones, and spatter landforms. Although this study represents only a subset of possible endmember small-volume mafic volcanic landforms, it demonstrates the feasibility and value of morphometric catalogs to remotely identify these landforms. Specifically, SMILES contains a larger number of simple maars and ring scoria cones and introduces a spectrum of collapse and spatter landform morphometrics to characterize each landform type. The catalog also helps to evaluate the appropriate size of study population needed for these characterizations considering the diversity of eruption histories recorded in small-volume volcanic landforms. The discrimination between similar-looking landforms, such as maars versus lava collapse features, that represent very different formation mechanisms is necessary to recognize first-order evidence of eruption styles providing valuable information to remote studies on volcanoes on Earth and other planetary surfaces. Martian volcanic landforms are often larger than terrestrial analogs with different cross-sectional morphologies (Brož et al., 2014). Therefore, the positive remote identification of volcanic landforms on other planets will require a diagnostic suite of dimensionless morphometric parameters along with qualitative contextual observations.

Previous works have shown that as the resolution of digital elevation models (DEMs) improves, the values and ranges of previously collected morphometric parameters can change and

warrant reassessment (Fornaciai et al., 2012; Vörös et al., 2021). This study leverages high-resolution (<0.1–5 m/pixel) DEM from unmanned aerial system (UAS) photogrammetry and OpenTopography, ArcticDEM, LiPAD, Oregon Department of Geology and Mineral Industries (DOGAMI), Instituto Nacional de Estadística Geografía y Informática (INEGI), and 3D Elevation Program (3DEP) open-source data repositories to develop a range of morphometric parameters from 20 simple maars, 22 lava collapse features, 24 spatter landforms, and 24 ring scoria cones to enable reproducible quantitatively informed remote identification of volcanic landforms.

## Methods

In this study, volcanic landforms are subdivided into two distinct groups, namely, negative volcanic landforms (NVLs) and positive volcanic landforms (PVLs). NVL are landforms that extend below the pre-eruptive surface, that is, maars and lava collapse features. PVLs build a constructive edifice above the pre-eruptive surface, that is, scoria cones and spatter landforms. Future iterations of SMILES will build on this foundation.

## Data sources

This study utilizes 69 digital elevation models (DEM) from both open-source data repositories (Harney Basin LiDAR by Oregon Department of Geology and Mineral Industries, 2015; Instituto Nacional de Estadística y Geografía (INEGI), 2021; OpenTopography, 2021; Porter et al., 2018; Sugarbaker et al., 2014) and data collected via uncrewed aerial system (UAS) photogrammetry (Nolan et al., 2019; Nolan and Graettinger, 2020). UAS data were processed using Agisoft Metashape. LiDAR datasets were rasterized using CloudCompare (CloudCompare 2.12.1, 2021). Spatial resolutions of the analyzed DEM range from 0.1 to 0.4 m/pixel for UAS data, 2 m/pixel for ArcticDEM, and 1–5 m/pixel for LiDAR data (Table 1, Supplementary Table S1 for more detail).

## Inclusion criteria

Landforms selected from SMILES are simple maars, lava collapse features, ring scoria cones, and spatter landforms. Maars and lava collapse features were constrained to ~2 km or less across the depression, and scoria cones and spatter landforms were constrained to a basal width of ~2 km or less and volumes less than 1 km<sup>3</sup>. This study focuses on basaltic monogenetic landforms resulting from a single eruption and dominated by a single eruption mechanism. Hence, multimodal landforms were not included in this study.

TABLE 1 Site list of current SMILES included landforms. This list does not include multimodal or complex landforms.

SMILES landform site	DEM spatial resolution (m/pixel)	# Of DEM	Analyzed landform	Landform type
Diamond Craters, Oregon, USA-UAS	0.1–0.4	12	17	SL,M,C
Diamond Craters, Oregon, USA-LiDAR	1	2	3	M
Hole in the Ground, Oregon, United States	1	1	1	M
Kileaua, Hawaii, United States	1	9	11	SL,C
Lunar Crater, Nevada, United States	1	1	1	M
El Malpais, New Mexico, United States	1	1	8	C,SC
Pinacate, Mexico	5	9	11	M,SC
Valle de Santiago, Mexico	5	5	4	M,SC
Xalapa Monogenetic V.F.	2	1	2	M
Laki, Iceland	2	11	12	SL
Askja, Iceland	1	4	7	SL
San Pablo (Laguna), Philippines	1	2	2	M
Bryce Canyon, Utah, United States of America	1	3	3	SC
Capulin, New Mexico, United States of America	1	1	1	SC
		69	90	

SL = Spatter landforms, M = Maars, C = Lava collapse features, SC = Scoria cones

Landforms were not selected if heavily vegetated, filled with water, or had an obvious human impact. All landforms had at least 75% of the original edifice/crater/depression intact to reduce misinterpretation of the shape and size. Desert environments were preferred to reduce impact of erosion. This study focuses on quaternary minimally altered simple small-volume monogenetic landforms from 13 sites in the United States, Iceland, Mexico, and the Philippines (Table 1).

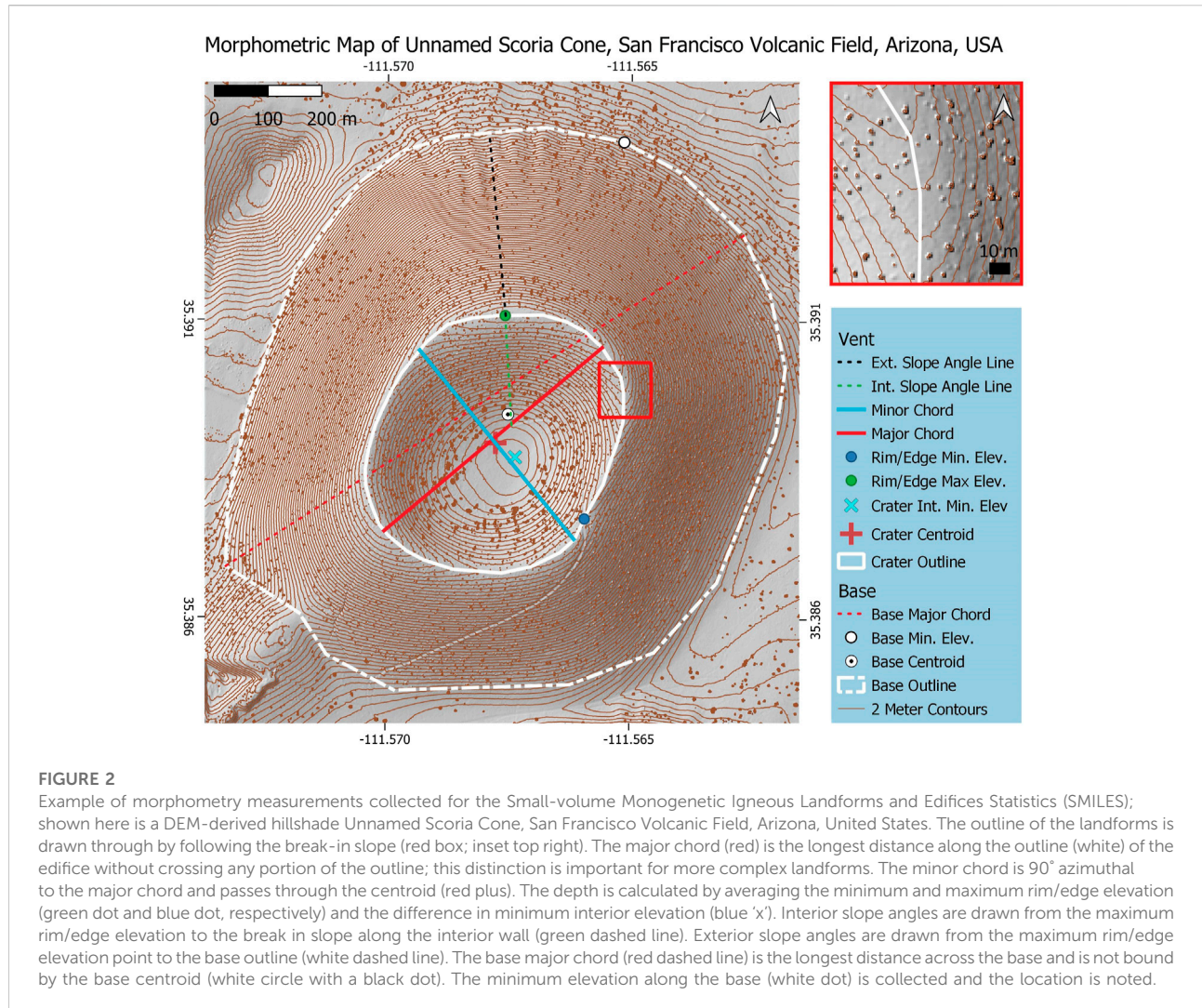
## Morphometry

The rims/edges of NVL were outlined using contour lines derived from DEMs in QGIS (QGIS.org, 2021) (Figure 2). Contour interval was chosen based on the overall landform size ranging from 0.25–2.5 m. The perimeter and area of the outline were calculated. The rim/edge outlines were quantified by the major chord (MChord), minor chord (mChord), and the centroid (Figure 2). The MChord is defined as the longest straight-line across the crater/depression/base outline without crossing any portion of the outline (Figure 2). For this study, the MChord is not required to pass through the centroid of the landform (Figure 2). The mChord crosses the MChord at 90° azimuth and passes through the centroid of the feature (Figure 2). The location of the minimum and maximum elevation along the outline of the rim/edge of each landform was located, as well as the minimum elevation inside the crater/depression (Figure 2). The average of min/max rim/edge elevation and minimum elevation is used to calculate the depth. The ejecta around the maar were not quantified here

because the exact extent of this distally thinning material can be extremely difficult to locate, and preservation is often limited. Additionally, the ejecta can extend up to 5 km from the maar (Lorenz, 2008), making collection *via* UAS not practical and LiDAR resolution (0.5–1 m/pixel) is too limited to identify the subtle changes in topography.

The craters of landforms of PVL were quantified like NVL depressions. The base of positive landform edifices was outlined using the break-in slope at the base of the landform (Figure 2). For this study, the term base is used to describe the outline of the cone and not the characteristics of the entire cone. From this outline, the base was quantified using the MChord, area, perimeter, and minimum elevation along the base outline (Figure 2). The depth of the crater/depression was calculated by the average rim/edge elevation and minimum internal elevation (Figure 2). The average rim/edge was used to derive the depth in order to remove a bias caused by the changes in surface topography for NVL.

Dimensionless parameters applied to the SMILES landforms include aspect ratio (AR), isoperimetric circularity (IC) (Graettinger, 2018), depth ratio (depth/MChord), MChord ratio (crater MChord/base MChord), crater to base area ratio (cArea/bArea), crater to base perimeter ratio (cPer/bPer), interior slope angle, and exterior slope angle. The aspect ratio is defined as the length of the mChord relative to the length of the MChord ( $AR = mChord/MChord$ ), which describes how equant a polygon is. The IC is the ratio between the area of the edifice outline and the area of a circle of the same perimeter ( $IC = 4\pi Area/Perimeter$ ). IC is a measure of variation in curvature of the outline, such that a perfect circle would have an IC of 1 and any variance would result in an IC < 1 (Graettinger, 2018). The interior angle inside the crater/depression was derived from the



point of max elevation along the rim/edge and location where the bottom begins to flatten out or the minimum interior elevation depending on the interior crater/depression morphology. The exterior slope angles were derived using a line starting at the maximum crater elevation location and running perpendicular to the crater outline to meet with the base outline. Depth ratio is the ratio of overall relief of a crater and its relation to the MChord of the crater ( $[\text{Max elev} - \text{Min Elev}] / \text{MChord}$ ).

## Results

Both NVL and PVL exhibit unique ranges of morphologies and morphometric parameters. However, simple maars and ring scoria cones have a narrower range of morphometric variability than lava collapse landforms and spatter landforms, respectively. Table 2 provides the ranges, means, and standard deviations (SD) of morphometric parameters.

## Negative landforms

Simple maar MChord lengths range from 73 to 2,046 m (mean = 802 m, SD = 637 m) with areas ranging from  $3 \times 10^3$  to  $2.4 \times 10^6 \text{ m}^2$ , and perimeters from 219 to 5,757 m. The AR of maars ranges from slightly elliptical (0.73) to circular (0.99) (mean = 0.9, SD = 0.06) (Table 2). The IC of simple maars ranges from 0.90 to 0.98, (mean = 0.96, SD = 0.02), reflecting smooth rim outlines. The depth of maars ranges from 8 to 438 m (mean = 94 m, SD = 103 m), with interior slope angles ranging from 14.9 to 47.1° (mean = 28.7°, SD = 7.3°) and depth ratios ranging from 0.03 to 0.26 (mean = 0.11, SD = 0.06). MChord topographic profiles of simple maars have an interior slope angle ( $<48^\circ$ ) with a smooth curving or flat bottom (Figure 3).

Lava collapse feature MChord lengths are 9–257 m (mean = 88 m, SD = 71 m), with areas between 49.2 and  $3 \times 10^4 \text{ m}^2$ , and perimeters ranging from 27 to 759 m. Lava collapse features can exhibit a near circular (0.95) to elliptic (0.26) aspect ratios

TABLE 2 SMILES database results.

	Maars	Lava collapse features	Spatter Landforms	Scoria cones
#	20	22	24	24
Major chord (m)	73–2,046 M=802 SD=637	9–257 M=88 SD=71	17–585 M=130 SD=122	64–531 M=253 SD=105
Aspect ratio	0.73–0.99 M=0.90 SD=0.06	0.26–0.95 M=0.66 SD=0.20	0.25–0.95 M=0.65 SD=0.21	0.54–0.96 M=0.83 SD=0.11
Area (m <sup>2</sup> )	$3.7 \times 10^3$ – $2.3 \times 10^6$	$4.9 \times 10^1$ – $3.5 \times 10^4$	$1.8 \times 10^2$ – $6.4 \times 10^4$	$2.6 \times 10^3$ – $1.8 \times 10^5$
Perimeter	$2.1 \times 10^2$ – $5.7 \times 10^3$	$2.7 \times 10^1$ – $7.6 \times 10^2$	$4.9 \times 10^1$ – $1.4 \times 10^3$	$1.9 \times 10^2$ – $1.5 \times 10^3$
Isoperimetric circularity	0.90–0.98 M=0.96 SD=0.02	0.46–0.98 M=0.79 SD=0.13	0.43–0.98 M=0.83 SD=0.16	0.81–0.99 M=0.95 SD=0.04
Interior slope angle (°)	14.9–47.1 M=28.7 SD=7.3	16.8–86.5 M=53.7 SD=25.8	11.3–63.1 M=31.0 SD=1.5	9.7–34.1 M=23.9 SD=5.6
Depth (m)	8–438 M=94 SD=103	4–19 M=11 SD=5	2–28 M=10 SD=7	9–79 M=34 SD=20
Depth ratio	0.03–0.26 M=0.11 SD=0.06	0.02–0.52 M=0.21 SD=0.13	0.04–0.37 M=0.11 SD=0.07	0.07–0.25 M=0.13 SD=0.05
Major chord (m)	-	-	29–634 M=177 SD=141	196–1,698 M=708 SD=334
Area (m <sup>2</sup> )	-	-	$6.1 \times 10^2$ – $9.2 \times 10^4$	$2.4 \times 10^4$ – $1.8 \times 10^6$
Perimeter (m)	-	-	$8.9 \times 10^1$ – $1.5 \times 10^3$	$5.6 \times 10^2$ – $4.9 \times 10^3$
Isoperimetric circularity	-	-	0.55–0.98 M=0.88 SD=0.10	0.85–0.98 M=0.94 SD=0.30
Exterior slope angle (°)	-	-	2.7–24.9 M=17.0 SD=7.2	10.2–30.3 M=23.7 SD=4.1
cArea/bArea	-	-	0.17–0.70 M=0.43 SD=0.13	0.06–0.27 M=0.15 SD=0.07
cPer/bPer	-	-	0.41–0.94 M=0.67 SD=0.12	0.26–0.53 M=0.37 SD=0.08
MChord ratio	-	-	0.43–0.92 M=0.70 SD=0.14	0.26–0.57 M=0.37 SD=0.08
Crater-base IC Diff	-	-	0.00–0.32 M=0.07 SD=0.08	0.00–0.09 M=0.03 SD=0.02

M=Mean SD = Standard Deviation.

(mean = 0.65, SD = 0.2). The IC of lava collapse features can reach high values (0.98) (Table 2), to complicated non-circular landform outlines (0.46) (mean = 0.79, SD = 0.13). Depths ranging from 4 to 19 m (mean = 11 m, SD = 5 m) with interior slope angles between 16.7 and 86.5° (mean = 53.7°, SD = 25.8) and depth ratios ranging 0.02–0.52 (mean = 0.21, SD = 0.13). Lava collapse features' topographic profiles exhibit a flat or saw-tooth bottom with interior slope angles, sometimes approaching 90° (Figure 3).

## Positive landforms

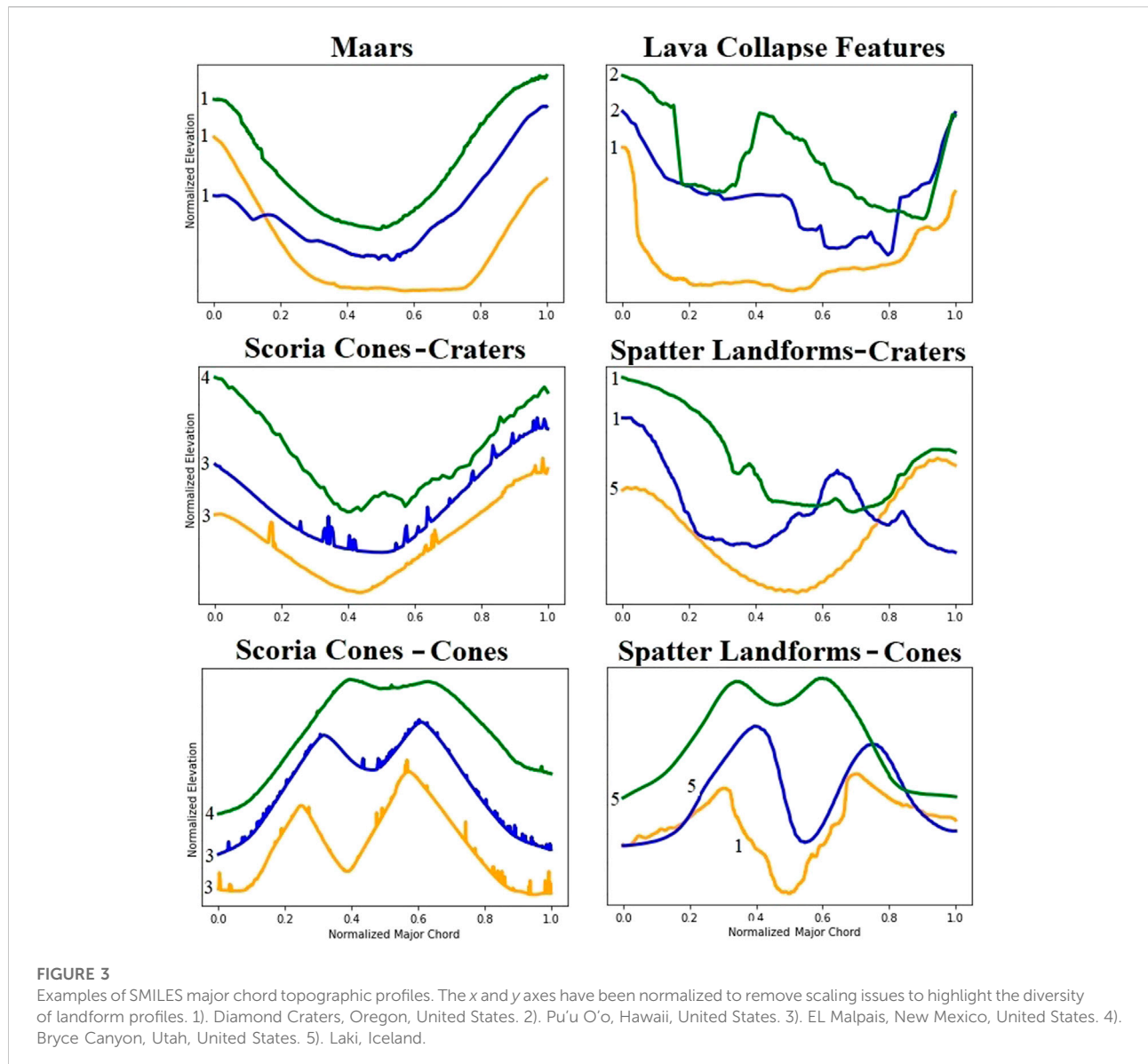
Spatter landform crater MChords range from 17 to 585 m (mean = 130 m, SD = 122 m), with areas ranging from 182 to  $6 \times 10^4$  m<sup>2</sup>, and perimeters ranging from 49 to 1,369 m. Spatter landform craters AR range from circular (0.95) to very elongate (0.25) (mean = 0.67, SD = 0.21). IC values range from non-circular (0.43) to smooth highly circular crater outlines (0.98) (mean = 0.84, SD = 0.16). The depth of spatter landform craters ranges from 2 to 28 m (mean = 10 m, SD = 7 m) with an interior angle of 11.3–63.1° (mean = 31.0°, SD = 11.5°), and depth ratios of 0.04–0.37 (mean = 0.11, SD = 0.07). Topographic profiles along the MChord of a spatter landform crater can range from a high angle relief reaching a mostly flat bottom with saw-tooth ridges to a smooth sloping rounded

bottom which can extend below the pre-existing surface (Figure 3). Spatter landforms often form in chains with lava flows directly emanating from the crater or proximally.

Spatter landform base MChords are 29–634 m (mean = 177 m, SD = 141 m), with areas ranging from 615 to  $9.2 \times 10^4$  m<sup>2</sup> and perimeters ranging from 89 to 1,461 m. The base IC ranges from non-circular (0.546) to smooth circular (0.98) in outline. Topographic profiles across the spatter landforms' edifice can range from smooth to hummocky/wavy (Figure 4). The spatter landform exterior slope angles are 2.7–24.9° (mean = 17.0°, SD = 7.2).

Scoria cone crater MChords range from 64 to 531 m (mean = 253 m, SD = 105 m) with areas between  $2.6 \times 10^3$  and  $1.8 \times 10^5$  m<sup>2</sup>, and perimeters ranging from 186 to 1,529 m. The scoria cone crater AR is between elongate (0.54) and circular (0.96) (mean = 0.82, SD = 0.11). IC values range from slightly non-circular (0.81) to circular (0.99) (mean = 0.95, SD = 0.04). The depth of scoria cone craters ranges from 9 to 79 m (mean = 34, SD = 20), has interior angles between 9.7 and 33.1° (mean = 23.9°, SD = 5.6°), and a depth ratio of 0.07–0.25 (mean = 0.13, SD = 0.05). Topographic profiles along the interior crater MChord have a smooth (<35°) slope to a rounded bottom (Figure 3). Scoria cones can be surrounded by or constructed on top of lava flows.

Scoria cone base MChords range from 196 to 1,698 m (mean = 708, SD = 334), with areas between  $2.3 \times 10^4$  and



$1.8 \times 10^7 \text{ m}^2$ , and perimeters ranging from 564 to 4,931 m. Base IC vary from nearing circular (0.85) to circular (0.98) (mean = 0.94, SD = 0.03). The topographic profile of a scoria cone edifice is smooth and often concave (Figure 4). Scoria cone exterior slope angles are  $10.2\text{--}30.3^\circ$  (mean =  $23.7^\circ$ , SD =  $4.1^\circ$ ).

## Discussion

Based on the morphometric measurements and dimensionless parameters collected in SMILES, the four studied mafic volcanic landform types can be represented by unique suites of diagnostic parameters. Although there are clear differences in the size of the studied landforms, the following discussion focuses on ratios that

are representative of the distinctive qualities of these landforms connected to the formation process that may be applicable to previously unknown features on Earth or other planets. The parameters are established based on comparisons of negative landforms that cut into the ground surface, and the positive landforms that construct an edifice.

### Negative landforms—remote classification

The morphological differences between lava collapse features and simple maars in SMILES are best demonstrated by the AR, IC, interior slope angle, and depth ratio. AR, IC, interior slope angle, and

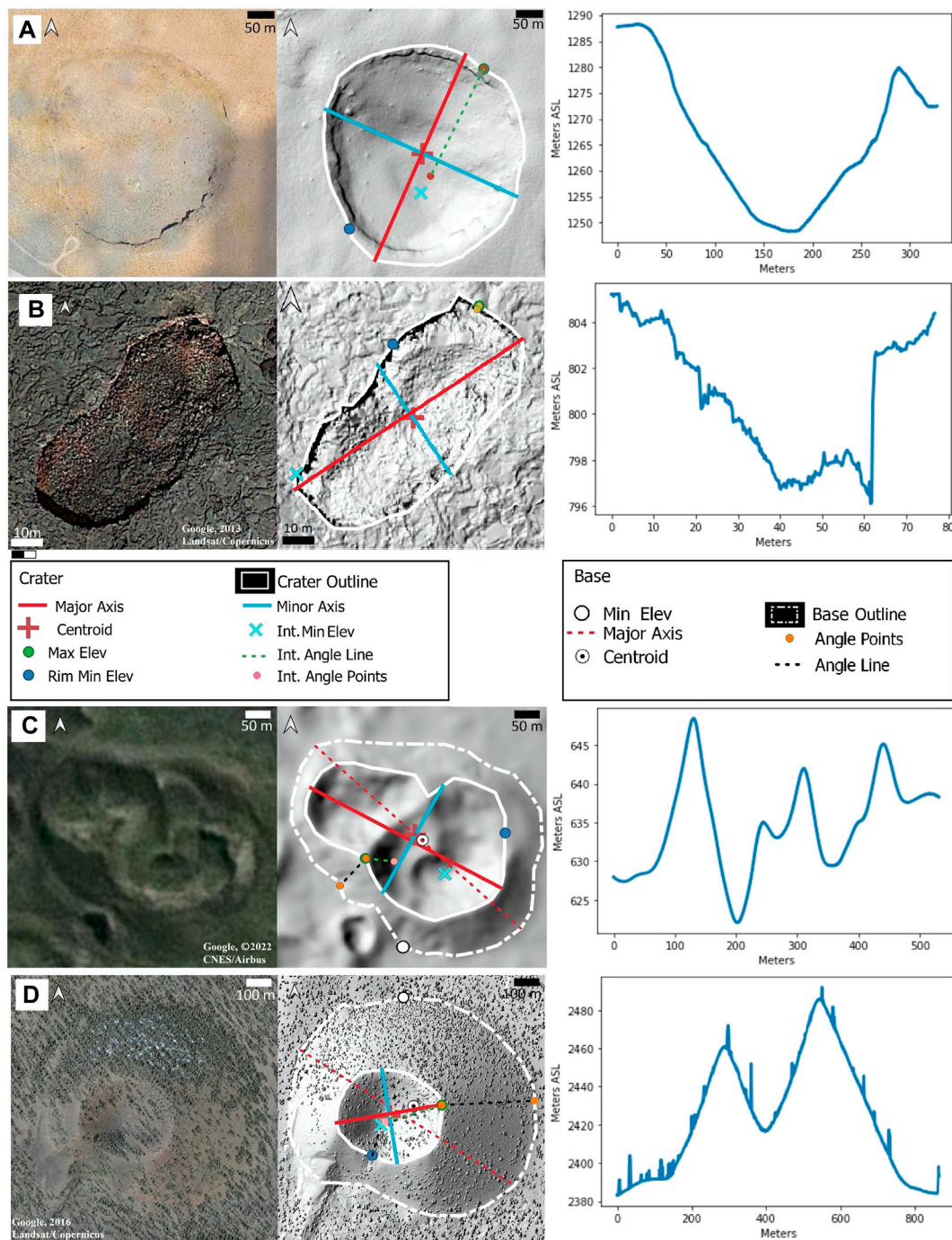


**FIGURE 4** Examples of SMILES landforms. (A) Aerial photography (left), DEM-derived hillshade (mid), and topographic profile (right) of West Twin Maar in Diamond Craters, Oregon, United States. (B) Lava collapse feature south of Pu'u 'O'o, Hawaii, United States. (C) Spatter landform in Laki, Iceland. (D) Unnamed scoria cone in El Malpais, New Mexico, United States. Visible spikes across the profile are caused by trees. The topographic profiles extend slightly beyond the landform outlines and follow the major chord for A and B, and the base major chord for C and D.

depth ratio of a simple maar fall within very distinct ranges (Figure 5). A simple maar is slightly elongated to near circular in 2D shape with smooth outlines and interior walls. The depth of

maars is shallow, and their depth ratio is low (table 2). The topographic profiles of maar MChord can have small zones of high relief due to the presence of resistant layers in the pre-existing

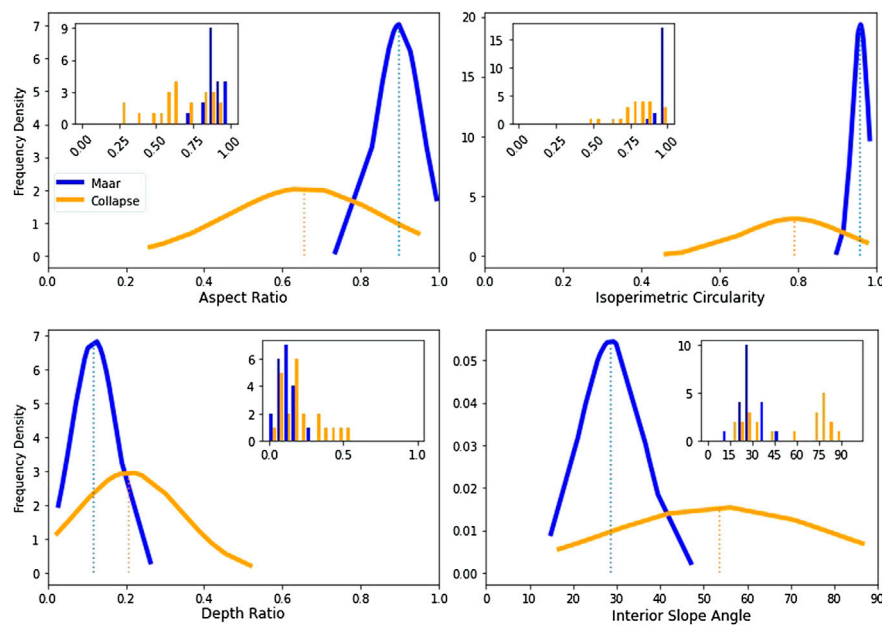


**FIGURE 5**

Frequency distribution of identified negative volcanic landforms parameters. Simple maars in this study ( $N = 20$ ) are a representative range of sizes and shapes from three continents. Maar parameters (blue) all fall in a very distinct range; aspect ratio  $>0.73$ , isoperimetric circularity  $>0.89$ , interior slope angle  $<47.7^\circ$ , and depth ratio  $<0.26$ . Collapse features ( $N = 22$ ) are representative sizes and shapes from three North American sites. Collapse features in this study are those formed by collapsed lava surfaces into a void. Collapse features morphometry parameters (orange) have a wider range variance; aspect ratio  $>0.26$ , isoperimetric circularity  $>0.46$ , interior slope angles  $<87^\circ$ .

bedrock, but the overall profile is broad or has a smooth transition to the rounded or flat bottom (Figures 3, 4). Often in DEM or satellite imagery, the pre-existing bedrock is visible inside the maar crater.

Qualitative field or image observations enable the identification of material types and contextual information can provide valuable support to the quantitative evaluation established earlier. For example, maars commonly appear in fields with other monogenetic volcanic landforms, such as Lunar Crater (Tadini et al., 2014; Valentine et al., 2017) or Diamond Craters (Peterson and Groh, 1964; Sherrod et al., 2012), or on/near the edifices of larger volcanoes, for example, Shishaldin (Stelling et al., 2002). Over 96% of quaternary maars globally occur in volcanic fields with other maars (Graettinger, 2018). The morphology of a maar is described as a crater with a rim that cuts into underlying topography (White and Ross, 2011). The challenge of qualitative identification of maars with such a simple definition is highlighted by individual examples in the SMILES database such as the Lava Pit Crater in DCOR that has an apparent rim comprised of lava flow and not ejecta (possibly a lava-rise pit), such that simply using the presence of a rim alone is not enough to classify a landform as a maar (Figure 6). The steep angled walls and saw-tooth bottom caused by the stacking of cooled lava plates seen in the Lava Pit Crater add additional context to classify it as a lava collapse feature.

The average AR and IC values in a lava collapse feature are below the minimum values found in simple maars. Although some lava

collapse features have the same AR and IC parameter values as a maar, highly symmetrical lava collapse features are not common (13% of population). It is important to note that IC is an exponential parameter, so a seemingly small deviation in IC means a significant loss in circularity (Figure 7). Lava collapse features have a saw tooth or flat bottom with higher depth ratios than maars and higher interior angles (Figures 3, 4). The interior slope of a lava collapse feature MChord can range from low to high angle but tends toward the higher angle endmembers (65% of collapse  $>40^\circ$ ) (Table 2). Small lava collapse features usually have the highest angle walls ( $>75^\circ$ ) (Figures 3, 4). Lava collapse features can occur as elongate structures and can be found often in chains. Lava collapse features in SMILES all occur in lava flow fields and are found near other volcanic landforms.

However, none of these parameters are individually diagnostic, the suite of parameters with supporting contextual information enables the discrimination of these two negative volcanic landforms. Unlike a lava collapse feature, simple maars have a narrow range of AR, IC, interior slope angle, and depth ratio. More complex maars with multiple overlapping depressions (Graettinger and Bearden, 2021) will require additional evaluation to determine the diagnostic parameter ranges and additional morphometric parameters. It is also worth noting that maars tend to be larger than lava collapse features; however, the emphasis of this study was to identify dimensionless parameters which translate to non-terrestrial landforms.

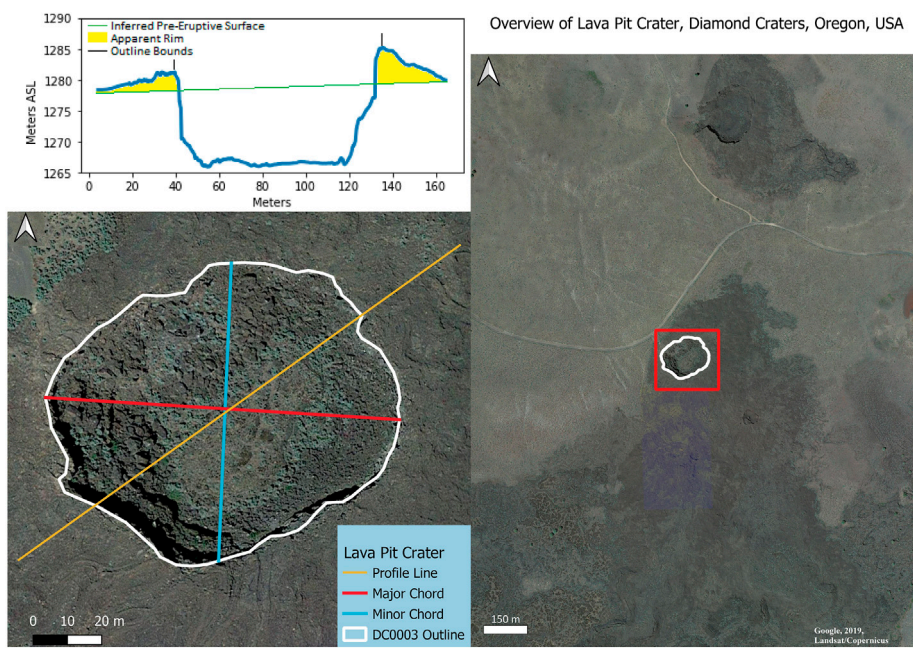


**FIGURE 6**  
 Extended topographic profile of Lava Pit Crater, Oregon, United States . This example is unique because it has an apparent rim; the presence of the rim alone is not solely diagnostic. Lava pit crater is lined with blocky cooled lava fragments. The interior slope angle is  $42.9^\circ$  with sections close to  $90^\circ$ . The bottom is flat or saw-toothed. The saw-tooth of this bottom is caused by large blocky cooled lava fragments. Vertical exaggeration = 2.5x.

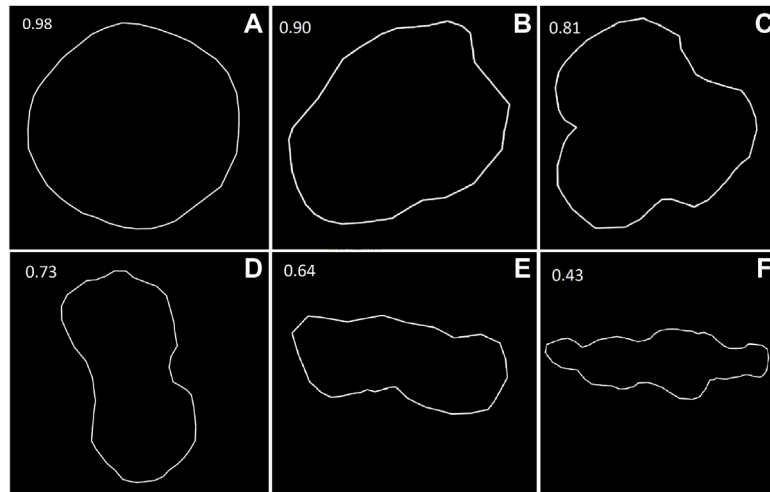
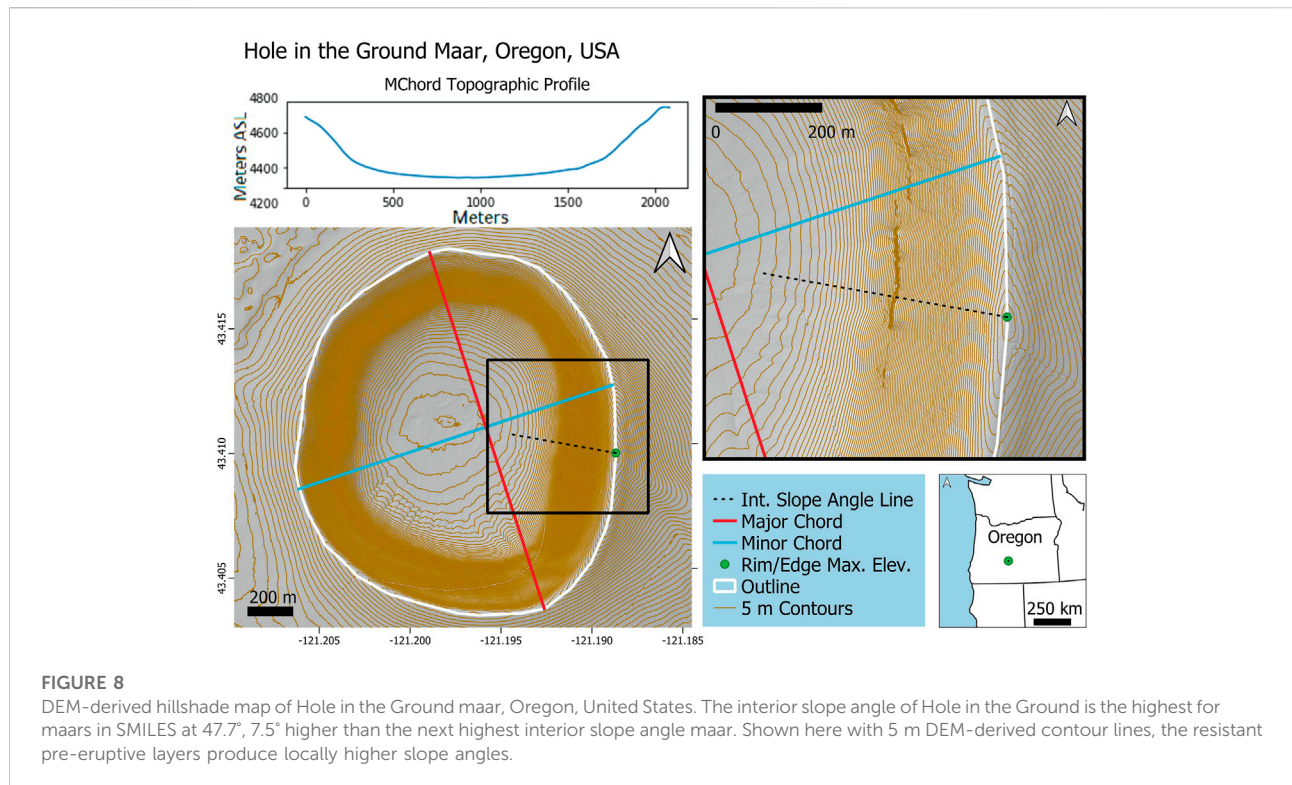


**FIGURE 7**  
 Changes in isoperimetric circularity (IC) from real examples. (A) Dry Maar, Diamond Craters, Oregon, United States. (B) DCOR-0012 unnamed maar, Diamond Craters, Oregon, United States. (C) Clover Maar, Diamond Craters, Oregon, United States. (D) DCOR-0009 collapse feature, Diamond Craters, Oregon, United States. (E) Laki-010 spatter landform, Laki, Iceland. (F) Laki-002, Laki, Iceland. Dry maar represents a circular outline (0.98) with Laki-002, a spatter landform, represents an elongate endmember (0.43). IC is an exponential parameter, thus a seemingly small change in value is a large change in overall circularity.



## Negative landforms—morphology controls

Maars are formed by an eruption that excavates the subsurface through a series of phreatomagmatic explosions that distribute a mixture of juvenile pyroclasts and fragmented country rock in a diatreme, crater, and ejecta ring (White and Ross, 2011). The morphology of the resulting crater relates to the fundamental formation mechanisms and the materials that define the landform rim/edge and interior. During the eruption, a maar will create ash to block/bomb-sized ejecta sourced from the pre-eruptive substrate and juvenile material. Although some material builds up the ejecta rim, much material returns to the crater (White and Ross, 2011; Valentine and White, 2012). This backfill process results in a landform that is covered in and built of loose debris at or below the angle of repose forming a smooth shallow crater (Figure 8; Table 2). Any high angles from individual large blocks or resistant units in the crater wall are commonly covered by ejecta resulting in a more subtle profile. Cases where the resistant bedrock still influences the average slope include Hole in the Ground, Oregon (Peterson and Groh, 1963) having the highest measured maar interior slope angle of 47.7° which is 7.5° higher than the next highest relief angle maar in SMILES (Figure 8). The process of multiple repeated explosions through a debris-filled crater contributes to the final shape of a maar by recycling crater fill and ejecta (Valentine and White, 2012; Graettinger et al., 2016; Macorps

et al., 2016) allowing gravitational processes to dominate the interior slope. Further evidence of the influence of this backfill debris on morphology was explored in large-scale experiments where closely spaced laterally migrating explosions still produced circular craters (Valentine et al., 2015; Graettinger and Bearden, 2021). There have also been studies of how maar craters degrade after the eruption where observations of Ukinrek maar in Alaska documented continued to fill with material from the rim through gravitational processes and an infilling lake (Pirring et al., 2008). These backfill processes leave a very distinctive profile, which coupled with AR, IC, interior slope angle, and depth ratio can be useful for the remote identification of a maar. Although maar external slopes were not quantified in this study due to the challenge of remotely delimiting the outer edge of ejecta even in well-preserved maars, the external slope angles are notably less than the angle of repose as a result of pyroclastic density currents that transport and deposit ejecta outside of the crater (White and Ross 2011; Graettinger and Valentine 2017).

Lava collapse features result from flowing lava that cools across the exposed surface creating a ‘roofed’ tube or channel (Kauahikaua et al., 1998). These channels may drain creating a hollow void and these roofs may collapse (Harris and Rowland, 2015). A common variety is lava tube skylights which can be seen on Earth, the Moon, and Mars (Sauro et al., 2020). Since the lava tubes and channels are created from flowing materials creating paths across land and other cooled lava flows (Peterson et al., 1994), a wide variety of oddly shaped and unsymmetrical

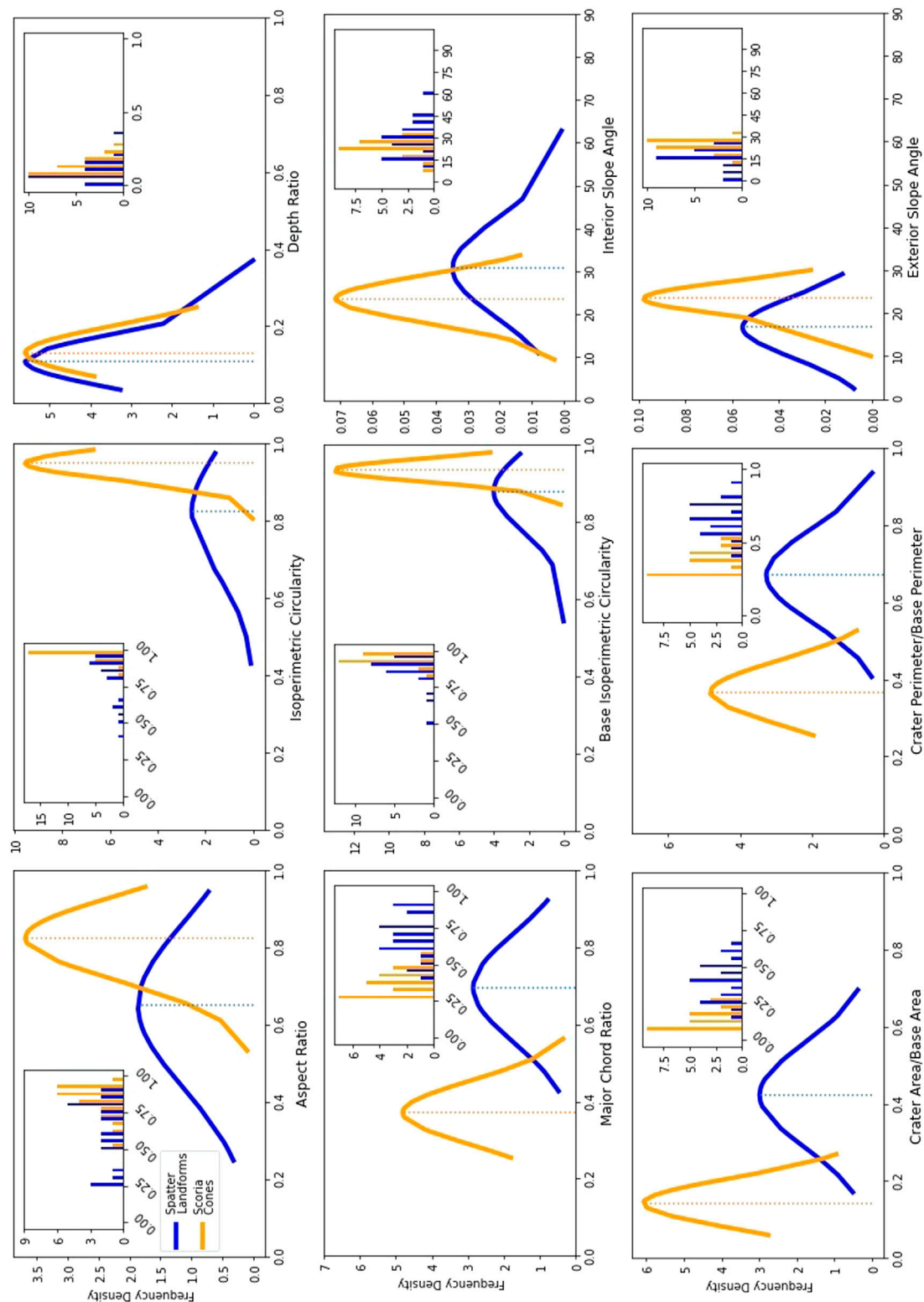


**FIGURE 9**

Frequency distribution of identified positive volcanic landforms parameters. The identified parameters for scoria cones all fall in a very distinct range. Spatter landforms have a wider variability of shapes. The  $cPer/bPer$ ,  $cArea/bArea$ , and flat-topped-ness of scoria cones represent a smaller vent relative to the base, while spatter landforms have a larger vent relative to the base.

channels are possible. Additionally, because lava collapse features can exhibit a lot of irregularities in shape, AR and IC have a broader range and these morphologies are preserved in the higher density/stronger materials (cooled lava). This higher density/stronger material allows for highly unsymmetrical morphometries to be maintained after formation. The resulting larger blocks can maintain a much higher angle of repose than pyroclastic material allowing higher interior slope angles in lava collapse feature relative to maars.

The low interior slope angle of NVL is related to a lower depth ratio. A rather shallow landform constrains the maximum interior slope angles (generally  $<40^\circ$ ) in maars. This lower depth ratio further suggests that the angle of repose and backfill processes are very important in the overall morphology of a maar eruption. Backfill processes of lava collapse features are slowed/stopped due to the higher strength materials and therefore can maintain a morphology with a higher depth ratio.

## Positive landforms—remote classification

The morphologic difference between spatter landforms and ring scoria cones is best demonstrated by IC, base IC, crater to base area ratio, crater to base perimeter ratio, crater MChord/base MChord ratio, crater depth ratio, and maximum interior slope angles (table 2). The crater IC, base IC, interior slope angle, and crater depth ratio of ring scoria cones have distinct, well-defined ranges (Figure 9). The measured interior slope angle of the scoria cones in SMILES agrees with the well-documented angle of repose ( $<40^\circ$ ) in scoria cones (e.g., Porter, 1972; Wood, 1980). The topographic profile of a scoria cone crater has shallow sloping walls ( $<35^\circ$ ) with a smooth transition to a rounded bottom, creating a bowl-shaped crater (Figures 3, 4).

The IC of a scoria cone's base is very close to the IC of the same cone's crater (average difference in same cone crater/base IC = 0.02, with a max difference of 0.09). Similar to the crater IC, the basal IC also has a distinct range (table 2). The scoria cones cArea/bArea, cPer/bPer, and MChord ratio represent a lower value range than spatter landforms. The MChord ratio is a similar parameter to the crater width/cone width ( $W_{cr}/W_{co}$ ), a common parameter in many studies, which relates the size of the crater to the size of the cone. Wood (1980) and Porter (1972) show an 'ideal cone'  $W_{cr}/W_{co}$  to be 0.40, and Fornaciai et al. (2012) found the average  $W_{cr}/W_{co}$  for 21 fields and 542 cones to range from 0.243 to 0.431. A topographic profile of a scoria cone base MChord has moderate slopes ( $<35^\circ$ ) with little to no variance in the exterior slope angle.

Scoria cones appear in large, distributed fields with other volcanic landforms, for example, Lunar Crater in Nevada (Valentine et al., 2017), or near/on larger volcanoes, such as Mauna Kea (Porter, 1972). Scoria cones can occur in the same field as spatter landforms, as well as other volcanic landforms. Scoria cones can also stand on top of or be the source of lava

flows, such as Paricutin (Krauskopf, 1948) and Lathrop Wells (Valentine et al., 2007). Scoria commonly exhibits a characteristic dark red color, though not solely diagnostic of scoria cones as spatter vents in Holuhraun (Voigt et al., 2021) exhibit the same color.

Measured spatter landform craters have a broader range of IC, AR, and interior slope angle than scoria cones (Figure 9). This broad range provides a baseline for future works on the diversity of spatter landform morphology. The parameters of a spatter landform crater can fall in the range of scoria cones, but the averages lie just at the higher/lower limits of the scoria cone range, except for the depth ratio which extends to both ends of the spectrum (Figure 9). Spatter landforms are often comprised of multiple concentric overlapping semi-, half, or full circles which result in the saw-tooth pattern across the topographic profile (Figures 3, 4, 10). Singular spatter landforms occur, such as DCOR-0028, and the MChord profile highly resembles that of a small maar with smooth sloping sides to a rounded bottom (Figures 3, 4), though the interior slope angles tend to be higher than a maar (up to  $63^\circ$ ). The spatter landform craters can breach the pre-eruptive surface as seen in the MChord topographic profile (Figure 3).

Spatter landform bases have a wide range of IC. Unlike a scoria cone, the IC of the spatter base can be less similar to the IC of the crater (average difference in same landform crater/base IC = 0.07, with a max difference of 0.32). The cArea/bArea, cPer/bPer, and major chord ratio of spatter landforms represent the higher values of the PVL spectrum and are representative of a larger crater relative to the base when corrected for scaling. The topographic profile of a spatter landform base can range from shallow to higher angles, but often has more dynamic interior and exterior slope variations than a scoria cone, sometimes with tiers that change the ascendant angle, which meets a rounded rim. The higher values of spatter landform crater to base ratios highlighted in this study, as well as the uniquely dynamic nature of the topographic profiles have not been previously described.

Scoria cone AR, IC, interior slope angle, and depth ratio have a narrow range of values in contrast to spatter landforms (Figure 9), similar to maars versus lava collapse features. The range of PVL crater/base parameters (cArea/bArea, cPer/bPer, and MChord ratio) have little overlap at the endmembers of each range and represent a difference in the relative basal size (Figure 9; Table 2). Again, while none of these parameters are solely diagnostic, the suite of parameters and qualitative observations allows for remote classification of these PVLs.

## Positive landforms—morphology controls

The main difference in the observed morphology of PVL in this study is caused by variance in explosivity and magma viscosity in the magmatic phases during eruption. Scoria cones are formed by the explosive fragmentation of low

viscosity magma with fountains reaching heights of a few hundred meters (Taddeucci et al., 2015), creating non-cemented, loose-packed scoria pyroclasts (e.g., Valentine and Gregg, 2008). These eruptions are driven by the gases already dissolved in the source magma, denoted as 'dry', rather than magma–water interactions (e.g., Cashman and Scheu, 2015). During the formation of the scoria cone, the explosivity can be Strombolian, Hawaiian, sub-Plinian, and anywhere in between (Fornaciai et al., 2012) with various phases of welded and non-welded pyroclasts of different sizes but the morphometry is heavily influenced by the dominance of loose pyroclastic material (McGetchin et al., 1974; Valentine et al., 2005; Mannen and Ito, 2007). The accumulation of loose vesicular pyroclasts around the vent is dictated by ballistic transport and to lesser a degree transport by wind (Valentine et al., 2005). The interior slopes of a scoria cone crater are dictated by the angle of repose of these particles creating a bowl-shaped profile, generally  $<40^\circ$ . Although the crater morphology of both scoria cones and maars are controlled by the angle of repose, the profile of maars often exhibits a minor change to a shallower angle near the bottom of the depression caused by the backfill of loose material (Figure 8) while a scoria cone crater has a semicircular profile without a flat bottom creating the characteristic bowl-like shape (Figures 3, 4).

Similarly, the external slope of a scoria cone is also dictated by the angle of repose (Table 2), unlike a maar where deposition includes dilute pyroclastic density currents that produce shallower slopes. As the scoria pile grows in height, the low cohesion of pyroclastic grains causes mobilization (Riedel et al., 2003; Mannen and Ito, 2007). The angle of repose for scoria cones ( $<40^\circ$ ) allows the pyroclasts to continually roll down the edifice as the cone grows. An increase in explosivity can lead the scoria base to grow more due to the increase in the aerial travel distance of ejected particles. If the vent is on a slope, pyroclasts interaction with the ground surface may cause a scoria cone base to grow elongate or form in other less circular configurations depending on the topography (Kereszturi et al., 2012; Grosse et al., 2020). Additionally, scoria cone base elongation can be associated with fracture and feeding dyke geometries (Tibaldi, 1995; Corazzato and Tibaldi, 2006). The angle of repose also forces the base to grow at such a rate that the crater is relatively small in comparison to the basal diameter ( $W_{cr}/W_{co} < 0.40$ ) (Wood, 1980).

Spatter landform craters are formed by low viscosity, low volatile content Hawaiian eruptions with phases of flowing and fountaining of lava (e.g., Rader and Geist, 2015). The viscosity of spatter is influenced by higher temperature and low silica (Sumner et al., 2005) and thus more fluid and ductile when landing than scoria. The more ductile spatter allows for cohesion, or agglutination, of the material which can cool at steeper angles and exhibit an irregular slope (Taddeucci et al., 2015) or even become mobile days after emplacement (Sumner, 1998). The more consolidated material does not backfill into the crater,

unlike a scoria cone, allowing the interior crater bottom to be at or possibly below the pre-existing surface, as seen in DCOR-0029 (Figure 3), though lava can pool in the area and fill the vent (Witt et al., 2018). The interior of a spatter landform crater can be a single circular crater leading to a MChord topographic profile which is bowl-shaped similar to a scoria cone, such as in DCOR-0028. The morphology of the spatter landform crater may also be described as multiple overlapping semi-, half, or full circles of cooled lava (Figure 10). The topographic profile across these overlapping circles is saw-toothed, but with smoother, more fluid nature than lava collapse features' sharper-angled 'tooth' (Figure 4, Figure 10).

Although this study showed that the exterior slope angle of a scoria cone and spatter landform overlap, spatter landforms in literature have been recognized to have steeper exterior angles than a scoria cone (Wood, 1980). Since the formation of the base is driven by a more fluid material, the underlying pre-existing topography will cause the sticky materials to shift and flow to cover surface (Parcheta et al., 2012). The base can flow creating a more circular base while the crater outline is scalloped or elongated. Although the vent itself may experience some variance in location, the molten materials may flow to a flat pre-existing topography allowing for pooling thus creating a circular base with a scalloped crater, see Laki (Reynolds et al., 2016) and the 1929 Askja spatter (Hartley et al., 2016) landforms. The denser, agglutinated materials have a higher angle of repose, the steeper angle walls resist backfill allowing the spatter landforms to have a higher MChord ratio, translating to a larger relative crater when compared to the same landforms base.

## Implications

Statistical comparisons of simple maars and ring scoria cones made in this study are calculated from a range of sizes, morphologies, and geologic regions of small-volume monogenetic volcanic landforms (Németh and Kereszturi, 2015; Bemis and Ferencz, 2017; Graettinger, 2018; Graettinger and Bearden, 2018). Using data acquired from the MaarVLS dataset (Graettinger and Bearden, 2018), 88% of maars have a major axis of 2,000 m or smaller ( $N=455$ ), of which 73% have an AR of 0.75 or greater, 69% have an IC of 0.90 or greater, and 61% meet both criteria ( $AR \geq 0.75$  and  $IC \geq 0.90$ ) ( $N=402$ ). A total of 13.1% of the scoria cones analyzed at Tenerife ( $N=297$ ) were classified as ring-shaped (Dóniz-Páez, 2015). Cross-analysis of these landforms would be vital in increasing the application of these parameters to natural examples. Unfortunately, the lack of a centralized publicly accessible database limits the analysis of scoria cone parameters.

As SMILES grows, the statistical trends exhibited by these endmembers from the current sampling range (maars  $N=20$ , scoria cones  $N=24$ ) are expected to shift with larger sample sizes. This study aimed to collect a representative range of sizes within the

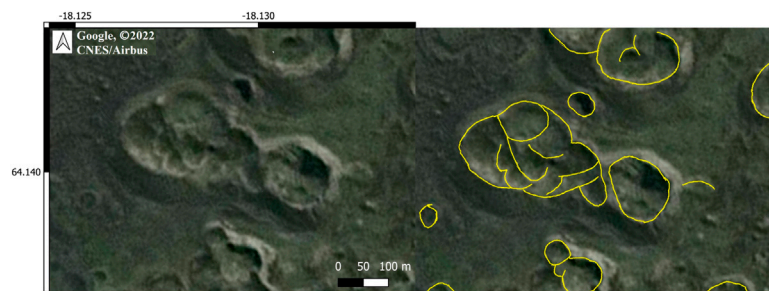


**FIGURE 10**

Spatter landforms (Laki, Iceland in this example) can be comprised of multiple layers of overlapping semi, half, and full circles.

pre-selected size limits ( $<2,000$  m and  $<1$  km<sup>3</sup>) to reduce the chance of major statistical changes, yet still anticipating only minor adjustments to the current numerical values. The parameters identified for simple maars and ring scoria cones represent a suite of diagnostic characteristics which increase the likelihood of accurate remote classification. The analysis of lava collapse landforms and spatter landforms provides a suite of parameters highlighting the diversity of these volcanic landforms. Further analysis of lava collapse features and spatter landforms is required to identify endmembers for cross analysis of the established simple maars and ring scoria cones.

This method can be applied to other landforms such as felsic lava domes, multimodal monogenetic landforms, more complex maars and scoria cones, and tuff rings. Catalogs like this are fundamental to establishing diagnostic characteristics of these features for remote identification on Earth and other planets. An emphasis was placed on identifying dimensionless parameters to allow for scaling between terrestrial and non-terrestrial landforms.

The representative parameters used for multimodal and compound landforms may vary from the less complex landforms investigated here. Other parameters measured that were not diagnostic for simple landforms are the distances/elevation changes between the MChord/mChord intersection location, the centroid, and the location of the minimum elevation, and how the previously mentioned parameters relate to overall landform asymmetry; however, these parameters may be more valuable when applied to more complex landforms.

SMILES is a growing and active catalog maintained by the authors. Additional DEM contributions to SMILES are welcomed. In addition to new landform types, SMILES would benefit from larger lava collapse features, more spatter landforms, and more complex scoria cones and maars to further refine the suites of diagnostic parameters for remote feature identification.

## Conclusion

SMILES is a catalog of morphometric parameters of simple maars, lava collapse features, spatter landforms, and ring scoria

cones. Currently, the growing SMILES catalog contains 177 small-volume mafic volcanic landforms, and this study highlights observations made on a subset of collected landforms. The landforms featured in this study cover a range of small-volume mafic volcanic landforms, providing a quantitative perspective on the morphometric properties of these landforms from 13 volcanic fields across three continents. This catalog represents a valuable tool for understanding the universal characteristics of these landforms across different volcanic fields.

The morphology of simple maars and ring scoria cones exhibits a narrow range of morphometric parameters. This narrow morphometric range places a quantitative boundary on these endmember landforms. Lava collapse features and spatter landforms require additional data and further analysis to quantify morphometric endmembers. Although no individual parameter is solely diagnostic, the suite of previously identified parameters paired with the novel parameters and observational context is fundamental to the characterization of volcanic landforms. Morphometric studies should also evaluate the geological context and visual observations to help support interpretations.

The most valuable parameters identified in this study are IC, depth ratio, and interior slope angle for NVL and interior angles, MChord ratios, and the crater/base area and perimeter ratios in PVL. SMILES reinforces the importance of using parameter suites derived from large populations of data for identifying the formation mechanisms remotely. Higher resolution data enable the collection of the detailed parameters needed for accurate remote classification. The results here indicate this approach could be applied to other landforms of volcanic and non-volcanic, terrestrial, and non-terrestrial origins.

Publicly available dataset repositories, such as Open Topography, INEGI, and ArcticDEM, are revolutionizing the way volcanologists can develop these critical catalogs to compare large varieties of landforms from around the globe. Additionally, SMILES can serve as a centralized, publicly

accessible dataset, which can aid other volcanologists and scientists in future studies.

## Data availability statement

The raw data supporting the conclusion of this article will be made available by the authors, without undue reservation.

## Author contributions

JN generated the bulk of the text, all the figures, and tables. AG contributed with text and editorial/correction.

## Funding

This project was partially funded by the Geological Society of America Graduate Research Grant, University of Missouri-Kansas City Newcomb Graduate Research Grant, and the Missouri Space Consortium.

## Acknowledgments

A very special thank you to ArcticDEM, OpenTopography, and INEGI, open repositories help

## References

- Aguilera, M., Ureta, G., Grosse, P., Németh, K., Aguilera, F., and Vilches, M. (2022). Geomorphological, morphometric, and spatial distribution analysis of the scoria cones in the Negros de Aras monogenetic volcanic field, northern Chile. *J. Volcanol. Geotherm. Res.* 422, 107458. doi:10.1016/j.jvolgeores.2021.107458
- Bemis, K. G., and Ferencz, M. (2017). Morphometric analysis of scoria cones: The potential for inferring process from shape. *Geol. Soc. Lond. Spec. Publ.* 446, 61–100. doi:10.1144/SP446.9
- Brož, P., Čadek, O., Hauber, E., and Rossi, A. P. (2014). Shape of scoria cones on Mars: Insights from numerical modeling of ballistic pathways. *Earth Planet. Sci. Lett.* 406, 14–23. doi:10.1016/j.epsl.2014.09.002
- Cañón-Tapia, E., and Walker, G. P. L. (2004). Global aspects of volcanism: The perspectives of “plate tectonics” and “volcanic systems. *Earth. Sci. Rev.* 66, 163–182. doi:10.1016/j.earscirev.2003.11.001
- Carracedo-Sánchez, M., Sarrionandia, F., Ábalos, B., Errandonea-Martin, J., and Gil Ibarra, J. I. (2017). Intra-cone plumbing system and eruptive dynamics of small-volume basaltic volcanoes: A case study in the calatrava volcanic field. *J. Volcanol. Geotherm. Res.* 348, 82–95. doi:10.1016/j.jvolgeores.2017.10.014
- Cashman, K. V., and Scheu, B. (2015). “Magmatic fragmentation,” in *The encyclopedia of volcanoes* (Elsevier), 459–471. doi:10.1016/B978-0-12-385938-9.00025-0
- Cloud Compare 2.12.1 (2021). *Cloud Compare 2.12.1*.
- Corazzato, C., and Tibaldi, A. (2006). Fracture control on type, morphology and distribution of parasitic volcanic cones: An example from Mt. Etna, Italy. *J. Volcanol. Geotherm. Res.* 158, 177–194. doi:10.1016/j.jvolgeores.2006.04.018
- Di Traglia, F., Cimarelli, C., de Rita, D., and Gimeno Torrente, D. (2009). Changing eruptive styles in basaltic explosive volcanism: Examples from Croscat

increase the value of already collected data and provide this data for no cost to download, allowing accessibility to all. We would like to thank the reviewers for their comments which helped strengthen this manuscript.

## Conflict of interest

The authors declare that the research was conducted in the absence of any commercial or financial relationships that could be construed as a potential conflict of interest.

## Publisher's note

All claims expressed in this article are solely those of the authors and do not necessarily represent those of their affiliated organizations, or those of the publisher, the editors, and the reviewers. Any product that may be evaluated in this article, or claim that may be made by its manufacturer, is not guaranteed or endorsed by the publisher.

## Supplementary material

The Supplementary Material for this article can be found online at: <https://www.frontiersin.org/articles/10.3389/feart.2022.910107/full#supplementary-material>

- complex scoria cone, Garrotxa Volcanic Field (NE Iberian Peninsula). *J. Volcanol. Geotherm. Res.* 180, 89–109. doi:10.1016/j.jvolgeores.2008.10.020
- Dóniz, J., Romero, C., Coello, E., Guillén, C., Sánchez, N., García-Cacho, L., et al. (2008). Morphological and statistical characterisation of recent mafic volcanism on Tenerife (Canary Islands, Spain). *J. Volcanol. Geotherm. Res.* 173, 185–195. doi:10.1016/j.jvolgeores.2007.12.046
- Dóniz-Páez, J. (2015). Volcanic geomorphological classification of the cinder cones of Tenerife (Canary Islands, Spain). *Geomorphology* 228, 432–447. doi:10.1016/j.geomorph.2014.10.004
- Fornaciai, A., Favalli, M., Karátson, D., Tarquini, S., and Boschi, E. (2012). Morphometry of scoria cones, and their relation to geodynamic setting: A DEM-based analysis. *J. Volcanol. Geotherm. Res.* 217–218, 56–72. doi:10.1016/j.jvolgeores.2011.12.012
- Graettinger, A., and Bearden, A. (2018). *Maar volcano location and shape (MaarVLS) database v 2.0*.
- Graettinger, A. H., and Bearden, A. T. (2021). Lateral migration of explosive hazards during maar eruptions constrained from crater shapes. *J. Appl. Volcanol.* 10, 3. doi:10.1186/s13617-021-00103-w
- Graettinger, A. H. (2018). Trends in maar crater size and shape using the global Maar Volcano Location and Shape (MaarVLS) database. *J. Volcanol. Geotherm. Res.* 357, 1–13. doi:10.1016/j.jvolgeores.2018.04.002
- Graettinger, A. H., Valentine, G. A., and Sonder, I. (2016). Recycling in debris-filled volcanic vents. *Geology* 44, 811–814. doi:10.1130/G38081.1
- Greeley, R., and Gault, D. E. (1979). “Endogenic craters on basaltic lava flows: Size frequency distributions,” in *Proc. Lunar planet. Sci. Conf.*, 2919–2933.
- Greeley, R. (1970). 1. Moon, 237–252. doi:10.1007/bf00562828 Terrestrial analogs to lunar dimple (drainage) craters *Moon*

- Grosse, P., Ochi Ramacciotti, M. L., Escalante Fochi, F., Guzmán, S., Orihashi, Y., and Sumino, H. (2020). Geomorphology, morphometry, spatial distribution and ages of mafic monogenetic volcanoes of the Peinado and Incahuasi fields, southernmost Central Volcanic Zone of the Andes. *J. Volcanol. Geotherm. Res.* 401, 106966. doi:10.1016/j.jvolgeores.2020.106966
- Harney Basin LiDAR by Oregon Department of Geology and Mineral Industries (2015). [WWW document]. URL Available at: [https://www.oregongeology.org/pubs/ldq/reports/2015\\_OLC\\_Harney\\_Basin\\_Data\\_Report.pdf](https://www.oregongeology.org/pubs/ldq/reports/2015_OLC_Harney_Basin_Data_Report.pdf).
- Harris, A. J. L., and Rowland, S. K. (2015). "Lava flows and rheology," in *The encyclopedia of volcanoes* (Elsevier), 321–342. doi:10.1016/B978-0-12-385938-9.00017-1
- Hartley, M. E., Thordarson, T., and de Joux, A. (2016). Postglacial eruptive history of the Askja region, North Iceland. *Bull. Volcanol.* 78, 28. doi:10.1007/s00445-016-1022-7
- Houghton, B. F., and Schmincke, H.-U. (1989). Rothenberg scoria cone, East eifel: A complex strombolian and phreatomagmatic volcano. *Bull. Volcanol.* 52, 28–48. doi:10.1007/BF00641385
- Instituto Nacional de Estadística y Geografía (INEGI) (2021). [WWW document]. URL Available at: <https://www.inegi.org.mx/programas/topografia/50000/>.
- Kauahikaua, J., Cashman, V., Mattox, N., Christina, C., Hon, A., Mangan, T., et al. (1998). Observations on basaltic lava streams in tubes from Kilauea volcano, island of Hawaii. *J. Geophys. Res.* 103, 27303–27323. doi:10.1029/97jb03576
- Kereszturi, G., Jordan, G., Németh, K., and Dóniz-Páez, J. F. (2012). Syn-eruptive morphometric variability of monogenetic scoria cones. *Bull. Volcanol.* 74, 2171–2185. doi:10.1007/s00445-012-0658-1
- Krauskopf, K. B. (1948). Mechanism of eruption at Paricutin volcano, Mexico. *Geol. Soc. Am. Bull.* 69, 711–732. doi:10.1130/0016-7606(1948)59[711:moeapv]2.0.co;2
- Lorenz, V. (2008). Explosive maar-diatreme volcanism in unconsolidated watersaturated sediments and its relevance for diamondiferous pipes. *Z. Dtsch. Gemmol. Ges.* 57, 41–60.
- Macorps, É., Graettinger, A. H., Valentine, G. A., Ross, P.-S., White, J. D. L., and Sonder, I. (2016). The effects of the host-substrate properties on maar-diatreme volcanoes: Experimental evidence. *Bull. Volcanol.* 78, 26. doi:10.1007/s00445-016-1013-8
- Mannen, K., and Ito, T. (2007). Formation of scoria cone during explosive eruption at Izu-Oshima volcano, Japan. *Geophys. Res. Lett.* 34, L18302. doi:10.1029/2007GL030874
- Martí, J., López, C., Bartolini, S., Becerril, L., and Geyer, A. (2016). Stress controls of monogenetic volcanism: A review. *Front. Earth Sci.* 4, 1–17. doi:10.3389/feart.2016.00106
- McGetchin, T. R., Settle, M., and Chouet, B. A. (1974). Cinder cone growth modeled after northeast crater, Mount Etna, Sicily. *J. Geophys. Res.* 79, 3257–3272. doi:10.1029/JB079i023p03257
- Murcia, H., and Németh, K. (2016). *Effusive monogenetic volcanism*. London: Intech Volcanoes, 13.
- Németh, K., and Kereszturi, G. (2015). Monogenetic volcanism: Personal views and discussion. *Int. J. Earth Sci.* 104, 2131–2146. doi:10.1007/s00531-015-1243-6
- Németh, K. (2010). "Monogenetic volcanic fields: Origin, sedimentary record, and relationship with polygenetic volcanism," in *What is a volcano?* (Boulder, CO: Geological Society of America), 43–66. doi:10.1130/2010.2470(04)
- Nolan, J., Bearden, A., Galletly, A., and Graettinger, A., 2019. *Quantifying morphometry through 3-d models produced BY UAV photogrammetry of volcanic craters and collapse features in Diamond Craters, Oregon and implications to Martian crater fields*. doi:10.1130/abs/2019AM-332779
- Nolan, J., and Graettinger, A. (2020). *Recognizing and quantifying diagnostic morphometric parameters for the remote identification of small volume volcanic landforms and related features*, 52. Boulder, CO: Geological Society of America Abstracts with Programs, 6. doi:10.1130/abs/2020AM-356423
- OpenTopography (2021). *Lunar Crater volcanic field, central Nevada* [WWW document]. La Jolla, CA: Distrib. by OpenTopography. doi:10.5069/G9PR7SX0
- Parcheta, C. E., Houghton, B. F., and Swanson, D. A. (2012). Hawaiian fissure fountains I: Decoding deposits—episode 1 of the 1969–1974 Mauna Ulu eruption. *Bull. Volcanol.* 74, 1729–1743. doi:10.1007/s00445-012-0621-1
- Peterson, D. W., Holcomb, R. T., Tilling, R. I., and Christiansen, R. L. (1994). Development of lava tubes in the light of observations at Mauna Ulu, Kilauea volcano, Hawaii. *Bull. Volcanol.* 56, 343–360. doi:10.1007/BF00326461
- Peterson, N., and Groh, E. A. (1964). *Ore bin/Oregon Geology magazine/journal*.
- Peterson, N. V., and Groh, E. A. (1963). *Maars of south-central Oregon*. Portland: ORE BIN, 25.
- Pirrung, M., Büchel, G., Lorenz, V., and Treutler, H.-C. (2008). Post-eruptive development of the Ukinrek East Maar since its eruption in 1977 A.D. in the periglacial area of south-west Alaska. *Sedimentology* 55, 305–334. doi:10.1111/j.1365-3091.2007.00900.x
- Porter, C., Morin, P., Howat, I., Noh, M.-J., Bates, B., Peterman, K., et al. (2018). *Arctic DEM* [WWW document]. Harvard Dataverse. doi:10.7910/DVN/OHHUKH
- Porter, S. C. (1972). Distribution, morphology, and size frequency of cinder cones on Mauna Kea volcano, Hawaii. *Bull. Geol. Soc. Am.* 83, 3607–3612. doi:10.1130/0016-7606(1972)83[3607:DMASFO]2.0.CO;2
- QGIS.org (2021). *QGIS geographic information system*.
- Rader, E., and Geist, D. (2015). Eruption conditions of spatter deposits. *J. Volcanol. Geotherm. Res.* 304, 287–293. doi:10.1016/j.jvolgeores.2015.09.011
- Reynolds, P., Brown, R. J., Thordarson, T., and Llewellyn, E. W. (2016). The architecture and shallow conduits of laki-type pyroclastic cones: Insights into a basaltic fissure eruption. *Bull. Volcanol.* 78, 36. doi:10.1007/s00445-016-1029-0
- Riedel, C., Ernst, G. G. J., and Riley, M. (2003). Controls on the growth and geometry of pyroclastic constructs. *J. Volcanol. Geotherm. Res.* 127, 121–152. doi:10.1016/S0377-0273(03)00196-3
- Russell, J. K., and Nicholls, J. (1987). Early crystallization history of alkali olivine basalts, Diamond Craters, Oregon. *Geochim. Cosmochim. Acta* 51, 143–154. doi:10.1016/0016-7037(87)90015-9
- Sauro, F., Pozzobon, R., Massironi, M., De Berardinis, P., Santagata, T., and De Waele, J. (2020). Lava tubes on Earth, Moon and Mars: A review on their size and morphology revealed by comparative planetology. *Earth. Sci. Rev.* 209, 103288. doi:10.1016/j.earscirev.2020.103288
- Sherrod, D. R., Champion, D. E., and McGeehin, J. P. (2012). Age and duration of volcanic activity at Diamond Craters, southeastern Oregon. *J. Volcanol. Geotherm. Res.* 247248, 108–114. doi:10.1016/j.jvolgeores.2012.08.008
- Smith, I. E. M., and Németh, K. (2017). Source to surface model of monogenetic volcanism: A critical review. *Geol. Soc. Lond. Spec. Publ.* 446, 1–28. doi:10.1144/SP446.14
- Stelling, P., Beget, J., Nye, C., Gardner, J., Devine, J. D., and George, R. M. M. (2002). Geology and petrology of ejecta from the 1999 eruption of Shishaldin Volcano, Alaska. *Bull. Volcanol.* 64, 548–561. doi:10.1007/s00445-002-0229-y
- Sugarbaker, L. J., Constance, E. W., Heidemann, H. K., Jason, A. L., Lukas, V., Saghy, D. L., et al. (2014). *The 3D elevation Program initiative — a call for action circular*, 1399. doi:10.3133/cir1399
- Sumner, J. M., Blake, S., Matela, R. J., and Wolff, J. A. (2005). *J. Volcanol. Geotherm. Res.* 142, 49–65. doi:10.1016/j.jvolgeores.2004.10.013
- Sumner, J. M. (1998). formation of clastogenic lava flows during fissure eruption and scoria cone collapse: The 1986 eruption of Izu-Oshima volcano, eastern Japan. *Bull. Volcanol.* 60, 195–212. doi:10.1007/s004450050227
- Taddeucci, J., Edmonds, M., Houghton, B., James, M. R., and Vergnolle, S. (2015). "Hawaiian and strombolian eruptions," in *The encyclopedia of volcanoes* (Elsevier), 485–503. doi:10.1016/B978-0-12-385938-9.00027-4
- Tadini, A., Bonali, F. L., Corazzato, C., Cortés, J. A., Tibaldi, A., and Valentine, G. A. (2014). Spatial distribution and structural analysis of vents in the Lunar Crater volcanic field (Nevada, USA). *Bull. Volcanol.* 76, 877. doi:10.1007/s00445-014-0877-8
- Tibaldi, A. (1995). Morphology of pyroclastic cones and tectonics. *J. Geophys. Res.* 100, 24521–24535. doi:10.1029/95JB02250
- Valentine, G. A., and Connor, C. B. (2015). "Basaltic volcanic fields," in *The encyclopedia of volcanoes*. Editors H. Sigurdsson, B. Houghton, S. McNutt, H. Rymer, and J. Styr (Amsterdam: Elsevier), 423–439. doi:10.1016/B978-0-12-385938-9.00023-7
- Valentine, G. A., Cortés, J. A., Widom, E., Smith, E. I., Rasoazanamparany, C., Johnsen, R., et al. (2017). Lunar Crater volcanic field (reveille and pancake ranges, basin and range province, Nevada, USA). *Geosphere* 13, 391–438. doi:10.1130/GES01428.1
- Valentine, G. A., Graettinger, A. H., Macorps, É., Ross, P.-S., White, J. D. L., Döhring, E., et al. (2015). Experiments with vertically and laterally migrating subsurface explosions with applications to the geology of phreatomagmatic and hydrothermal explosion craters and diatremes. *Bull. Volcanol.* 77, 15. doi:10.1007/s00445-015-0901-7

- Valentine, G. A., and Gregg, T. K. P. (2008). Continental basaltic volcanoes — processes and problems. *J. Volcanol. Geotherm. Res.* 177, 857–873. doi:10.1016/j.jvolgeores.2008.01.050
- Valentine, G. A., Krier, D. J., Perry, F. V., and Heiken, G. (2007). Eruptive and geomorphic processes at the Lathrop Wells scoria cone volcano. *J. Volcanol. Geotherm. Res.* 161, 57–80. doi:10.1016/j.jvolgeores.2006.11.003
- Valentine, G. A., Krier, D., Perry, F. V., and Heiken, G. (2005). Scoria cone construction mechanisms, Lathrop Wells volcano, southern Nevada, USA. *Geology* 33, 629–632. doi:10.1130/G21459AR.1
- Valentine, G. A., Ort, M. H., and Cortés, J. A. (2021). Quaternary basaltic volcanic fields of the American Southwest. *Geosph. (Boulder)* 17, 2144–2171. doi:10.1130/GES02405.1
- Valentine, G. A., Perry, F. V., Krier, D., Keating, G. N., Kelley, R. E., and Cogbill, A. H. (2006). Small-volume basaltic volcanoes: Eruptive products and processes, and post-eruptive geomorphic evolution in Crater Flat (Pleistocene), southern Nevada. *Geol. Soc. Am. Bull.* 118, 1313–1330. doi:10.1130/B25956.1
- Valentine, G. A., and White, J. D. L. (2012). Revised conceptual model for maar-diatremes: Subsurface processes, energetics, and eruptive products. *Geology* 40, 1111–1114. doi:10.1130/G33411.1
- Vespermann, D., and Schmincke, H.-U. (2000). “Scoria cones and tuff rings,” in *Encyclopedia of volcanoes*. Editor H. Sigurdsson (San Diego: Academic Press), 683–694.
- Voigt, J. R. C., Hamilton, C. W., Scheidt, S. P., Münzer, U., Höskuldsson, Á., Jónsdóttir, I., et al. (2021). Geomorphological characterization of the 2014–2015 Holuhraun lava flow-field in Iceland. *J. Volcanol. Geotherm. Res.* 419, 107278. doi:10.1016/j.jvolgeores.2021.107278
- Vörös, F., de Vries, B. van W., Karátson, D., and Székely, B. (2021). DTM-based morphometric analysis of scoria cones of the chaîne des puys (France)—The classic and a new approach. *Remote Sens. (Basel)* 13, 1983. doi:10.3390/rs13101983
- White, J. D. L., and Ross, P.-S. (2011). Maar-diatreme volcanoes: A review. *J. Volcanol. Geotherm. Res.* 201, 1–29. doi:10.1016/j.jvolgeores.2011.01.010
- Witt, T., Walter, T. R., Müller, D., Guðmundsson, M. T., and Schöpa, A. (2018). The relationship between lava fountaining and vent morphology for the 2014–2015 Holuhraun eruption, Iceland, analyzed by video monitoring and topographic mapping. *Front. Earth Sci.* 6, 235. doi:10.3389/feart.2018.00235
- Witt, T., and Walter, T. R. (2017). Video monitoring reveals pulsating vents and propagation path of fissure eruption during the March 2011 Pu’u ’Ō’ō eruption, Kīlauea volcano. *J. Volcanol. Geotherm. Res.* 330, 43–55. doi:10.1016/j.jvolgeores.2016.11.012
- Wood, C. A. (1980). Morphometric evolution of cinder cones. *J. Volcanol. Geotherm. Res.* 7, 387–413. doi:10.1016/0377-0273(80)90040-2